Characterization of Lipid Bilayers and Protein Assemblies Supported on Rough Surfaces by Atomic Force Microscopy†

Ralf P. Richter and Alain Brisson*

Laboratoire d'Imagerie Moléculaire et Nano-Bio-Technologie, IECB, Université Bordeaux I, 16 Avenue Pey Berland, 33607 Pessac Cedex, France

Received August 19, 2002. In Final Form: November 12, 2002

Supported lipid bilayers (SLBs) and two-dimensional protein assemblies formed on solid supports of various roughnesses were characterized by atomic force microscopy (AFM). The presence of SLBs was detected reliably by force measurements and by imaging. Three types of responses could be distinguished depending on the applied loads. These responses are interpreted as due to transient restructuration of the lipid assembly in the region of contact between lipid-covered support and AFM tip, driven by hydrophobic/hydrophilic interactions. Two-dimensional crystals of streptavidin could be resolved on SLBs formed on silicon wafers, whereas annexin A5, previously shown to crystallize on mica-SLBs, formed a close-packed noncrystalline assembly on lipid bilayers supported by silicon wafers.

Introduction

Atomic force microscopy (AFM) is recognized for its potential in providing a diversity of information such as topography, elastic properties, and interaction forces, in liquids, at supramolecular and submolecular levels. An important limitation of topography studies by AFM is its requirement for flat surfaces. The resolution of AFM images is indeed limited due to tip-convolution effects.[1,2] The use of rough surfaces would increase the difficulties in extracting the signal of the adsorbent in the recorded topography. In addition, increased tip−sample interactions would risk enhancing mechanical damage on soft samples. This explains why AFM imaging studies are usually performed on atomically flat surfaces, such as mica or highly oriented pyrolytic graphite (HOPG).[3−6] The characterization of biomolecules by force spectroscopy[7,8] is though not limited to flat surfaces.

On the other hand, most substrates with (bio)chemical properties of interest for fundamental research and biotechnological applications are difficult or impossible to render atomically flat. In particular, surface sensitive methods such as quartz crystal microbalance with dissipation monitoring (QCM-D), surface plasmon resonance, or ellipsometry, commonly used to investigate adsorption processes, require surfaces that are not atomically flat, for example, gold, sputtered silica, or silicon wafers (despite some recent progress[9]).

Next to other physicochemical properties of surfaces which are determinants for the adsorption of biomolecules and the conformational state of the adsorbent, such as their chemical nature, charge, hydrophilicity, or structure, the role of surface roughness in adsorption phenomena is poorly characterized. Roughness imposes local geometrical constraints on the adsorbents which can be crucial for self-assembly processes, particularly when the sizes of self-assembled domains exceed the characteristic dimensions of the surface features. Thus, roughness is expected to influence the formation and organization of self-assembled biomolecular systems such as supported lipid bilayers (SLBs)[10] or two-dimensional (2D) crystals of proteins.[11]

The objective of this study was to evaluate the possibilities of the AFM technique to characterize adsorption phenomena on solid supports of various roughnesses. We focused on two model systems, SLBs and 2D crystals of proteins, grown on SLBs, for their potential interest as biocompatible surfaces. Vesicles with a lipid composition of dioleoylphosphatidylcholine (DOPC)/dioleoylphosphatidylserine (DOPS) (molar ratio 4:1) were chosen as they form essentially defect-free SLBs as shown by AFM on flat mica surfaces[12] and by QCM-D on rough surfaces.[13] The proteins streptavidin[14] and annexin A5[6,15] were also previously shown to self-assemble into 2D crystals on mica-SLBs.

The literature on lipid assemblies deposited on solid supports and investigated by AFM is extensive.[2,16] While

* Corresponding author. Phone: +33 5 57 96 34 58. Fax: +33 5 57 96 34 84. E-mail: a.brisson@iecb-polytechnique.u-bordeaux.fr.

† Part of the *Langmuir* special issue entitled The Biomolecular Interface.

(1) Engel, A.; Schoenenberger, C.-A.; Müller, D. J. *Curr. Opin. Struct. Biol.* **1997**, *7*, 279−284.
(2) Shao, Z.; Mou, J.; Czajkowsky, D. M.; Yang, J.; Yuan, J.-Y. *Adv. Phys.* **1996**, *45*, 1−86.
(3) Scheuring, S.; Müller, D. J.; Ringler, P.; Heymann, J. B.; Engel, A. *J. Microsc.* **1999**, *193*, 28−35.
(4) Müller, D. J.; Fotiadis, D.; Engel, A. *FEBS Lett.* **1998**, *430*, 105−111.
(5) Scheuring, S.; Stahlberg, H.; Chami, M.; Houssin, C.; Rigaud, J.-L.; Engel, A. *Mol. Microbiol.* **2002**, *44*, 675−684.
(6) Reviakine, I.; Bergsma-Schutter, W.; Brisson, A. *J. Struct. Biol.* **1998**, *121*, 356−361.
(7) Rief, M.; Gautel, M.; Oesterhelt, F.; Fernandez, J. M.; Gaub, H. E. *Science* **1997**, *276*, 1109−1112.
(8) Rief, M.; Clausen-Schaumann, H.; Gaub, H. E. *Nat. Struct. Biol.* **1999**, *6*, 346−349.
(9) Benes, M.; Billy, D.; Hermens, W. T.; Hof, M. *Biol. Chem.* **2002**, *383*, 337−341.
(10) Rädler, J.; Strey, H.; Sackmann, E. *Langmuir* **1995**, *11*, 4539−4548.
(11) Brisson, A.; Bergsma-Schutter, A.; Oling, F.; Lambert, O.; Reviakine, I. *J. Cryst. Growth* **1999**, *196*, 456−470.
(12) Reviakine, I.; Brisson, A. *Langmuir* **2000**, *16*, 1806−1815.
(13) Richter, R.; Mukhopadhay, A.; Brisson, A. *Biophys. J.* **2002**, submitted.
(14) Reviakine, I.; Brisson, A. *Langmuir* **2001**, *17*, 8293−8299.
(15) Reviakine, I.; Bergsma-Schutter, W.; Mazères-Dubut, C.; Govorukhina, N.; Brisson, A. *J. Struct. Biol.* **2000**, *131*, 234−239.
(16) Dufrêne, Y. F.; Lee, G. U. *Biochim. Biophys. Acta* **2000**, *1509*, 14−41.

10.1021/la026427w CCC: $25.00
Published on Web 01/09/2003

many studies performed on mica were mostly descriptive and information on the distribution of fluid-phase and solid-phase domains in lipid mixtures[2,17,18] or the transition from vesicles to bilayer disks[12] could be obtained by using contact mode AFM at lowest force, the critical influence of the tip−sample interactions in the case of lipid systems has been identified with the exemplary water-skiing effect reported by Rädler et al.[19] Mechanical interactions between tip and SLBs and their influence on the imaging of SLBs has since been addressed in several publications measuring normal[20,21] and lateral (friction)[22,23] forces. Jumps on bilayers have frequently been reported and have been interpreted as a breakthrough of the tip in the bilayer.[21,22]

In this paper, tools to characterize SLBs on rough surfaces are presented. As for studies with flat surfaces, an understanding of the interaction between tip and bilayer is important for the interpretation of the data.

Materials and Methods

Materials. DOPC and DOPS were purchased from Avanti Polar Lipids (AL). *N*-(6-((Biotinoyl)aminohexanoyl-dipalmitoylphosphatidylethanolamine, triethylammonium salt (DPPE-lc-biotin), was purchased from Pierce (IL). Recombinant rat annexin A5 was overexpressed in *Escherichia coli*.[15] Lyophilized streptavidin and other chemicals were purchased from Sigma. Ultrapure water with a resistivity of 18.2 MΩ was used, prepared with a Maxima system (USF ELGA, France).

Muscovite mica plates of 11 mm diameter were purchased from Metafix (Montdidier, France). Plates of (11 × 11) mm^2 of pure silicon wafer and wafers thermally coated with 500 nm of silica were provided by the CEA (Grenoble, France). QCM-D sensor crystals, covered with 100 nm of evaporated gold and reactively sputter-coated with 50 nm silicon oxide, were purchased from Q-Sense (Gothenburg, Sweden).

A buffer solution made of 150 mM NaCl, 2 mM NaN_3, and 10 mM HEPES, pH 7.4, was prepared in ultrapure water, and 2 mM EDTA or $CaCl_2$ was added as indicated in the text. Streptavidin was resuspended in EDTA-containing buffer at 1 mg protein per mL.

Lipid Vesicle Preparation. Lipids were dissolved in chloroform, mixed in desired amounts, dried under a stream of nitrogen followed by drying in a vacuum desiccator overnight, resuspended at 1−2 mg/mL final concentration, and vortexed in EDTA-containing buffer. Lipid mixtures were homogenized by five cycles of freeze−thawing and subsequent vortexing. Small unilamellar vesicles (SUVs) were obtained by sonication with a tip-sonicator (Misonix, NY) operated in a pulsed mode at 30% duty cycle for 30 min with refrigeration, followed by centrifugation in an Eppendorf centrifuge (10 min at 16 000*g*) to remove titanium particles. SUV suspensions were stored at 4 °C under nitrogen and used within 4 weeks.

Support Preparation. Mica disks were glued to Teflon-coated (Bytac, Norton) metal disks using a two-component epoxy glue. Uniform surfaces were obtained by cleavage with Scotch tape and immediately covered with buffer solution.

Silica and silicon substrates were cleaned by two cycles of exposure to 2% sodium dodecyl sulfate (SDS) solution for 15 min, rinsing with ultrapure water, blow-drying with nitrogen, and exposure to UV/ozone for 10 min. For UV/ozone treatment, the substrates were placed in the vicinity of a mercury grid lamp (BHK, CA), mounted into a home-built chamber and driven by a suitable power source (BHK). Ozone is produced from the oxygen present in ambient air by the emitted UV light of wavelength 185 nm. By this treatment, the surface is cleaned from traces of organic contaminants[24] and rendered hydrophilic.[25] Substrates cleaned in this way were stored in air. Prior to use, they were re-exposed to UV/ozone for 10 min, attached to Teflon-coated metal disks using double-sided tape (Tesa, Hamburg, Germany), and immediately covered with buffer solution.

For simplicity, UV/ozone-treated silicon wafers will hereafter be referred to as "silicon wafers". Note, however, that due to exposure to oxygen in ambient air and due to the UV/ozone treatment, these wafers are covered by an oxide layer that is several nanometers thick.[24] Thermally silica-coated wafers and silica-coated QCM-D sensor crystals will be referred to as "silica-coated wafers" and "silica-coated quartz crystals", respectively.

Sample Preparation. If not stated otherwise, substrates were covered by 100 μL of calcium-containing buffer to which a SUV suspension was added at 0.1 mg/mL final concentration. After 30 min of exposure, vesicles present in solution were removed by cycles of exchange of the lipid solution with buffer solution, by pipetting.

Atomic Force Microscopy. AFM measurements were performed in liquid using a Nanoscope IV-Multimode (Veeco, Dourdan, France), equipped with a J-scanner (120 μm). The contact mode fluid cell was washed by sonication in subsequent baths of ethanol and ultrapure water, followed by extensive rinsing in ethanol and blow-drying in a stream of argon. Tubings were sonicated in ethanol and water and rinsed with water. The O-ring was rinsed with water. Oxide-sharpened silicon nitride cantilevers with nominal spring constants of 0.06 and 0.32 N/m (Digital Instruments, CA) were exposed to UV/ozone (BHK) for 10 min prior to use. The spring constants were recalibrated using the unloaded resonant frequency.[26]

The liquid-covered substrates were installed in the AFM cell using the O-ring and rinsed with 1 mL of buffer. The AFM was equilibrated for 1 h prior to imaging. Sample solution or buffer was injected with a syringe when necessary.

Images acquired in constant force contact mode were recorded at a scanning rate of 4−8 Hz and a scan angle of 90°. Images were flattened and plane-fitted except when otherwise stated. Roughness values given are root-mean-square (rms) values determined from (500 × 500) nm^2 images, if not otherwise stated.

Contact mode force−displacement curves were acquired at approach and retraction speeds of 350 nm/s (unless otherwise stated) and converted to force−distance plots.[27] Repulsive and adhesive forces are denoted with positive and negative signs, respectively. Friction data were obtained by subtracting friction images recorded in trace and retrace, which averages out irregularities due to surface roughness.[23] Values are given in millivolts corresponding to the response of the photodiode, which is assumed to be proportional to the friction force.

Results

Lipid Bilayers on Solid Supports. Solid supports and substrates covered with SLBs of DOPC/DOPS (molar ratio 4:1) were characterized in calcium-containing buffer by imaging in contact mode and by force−distance curves.

Imaging Solid Supports. The surface roughness of the solid supports used in this study (mica, silicon wafer, silica-coated wafer, and silica-coated quartz crystal) was characterized by contact mode AFM. On mica, no corrugations were discernible, the surface being flat over areas larger than (10 × 10) μm^2 (not shown) and exhibiting a surface roughness of less than 0.05 nm, considered as the noise limit of our equipment. Silicon wafers (Figure 1A) were essentially flat on scales of 50 nm and larger but showed surface features of subnanometer height and lateral

(17) Rinia, H. A.; Kruijff, B. D. *FEBS Lett.* **2001**, *504*, 194−199.
(18) Reviakine, I.; Simon, A.; Brisson, A. *Langmuir* **2000**, *16*, 1473−1477.
(19) Rädler, J.; Radmacher, M.; Gaub, H. E. *Langmuir* **1994**, *10*, 3111−3115.
(20) Franz, V.; Loi, S.; Müller, H.; Bamberg, E.; Butt, H.-J. *Colloids Surf., B* **2002**, *23*, 191−200.
(21) Müller, H.; Butt, H.-J.; Bamberg, E. *J. Phys. Chem. B* **2000**, *104*, 4552−4559.
(22) Schneider, J.; Dufrêne, Y. F.; Barger, W. R., Jr.; Lee, G. U. *Biophys. J.* **2000**, *79*, 1107−1118.
(23) Grant, L. M.; Tiberg, F. *Biophys. J.* **2002**, *82*, 1373−1385.
(24) Vig, J. R. In *Treatise on Clean Surface Technology*; Mittal, K. L., Ed.; Plenum Press: New York, 1987; Vol. 1, p 1−26.
(25) Keller, C. A.; Kasemo, B. *Biophys. J.* **1998**, *75*, 1397−1402.
(26) Cleveland, J. P.; Manne, S.; Bocek, D.; Hansma, P. K. *Rev. Sci. Instrum.* **1993**, *64*, 403−405.
(27) Mueller, H.; Butt, H.-J.; Bamberg, E. *Biophys. J.* **1999**, *76*, 1072−1079.

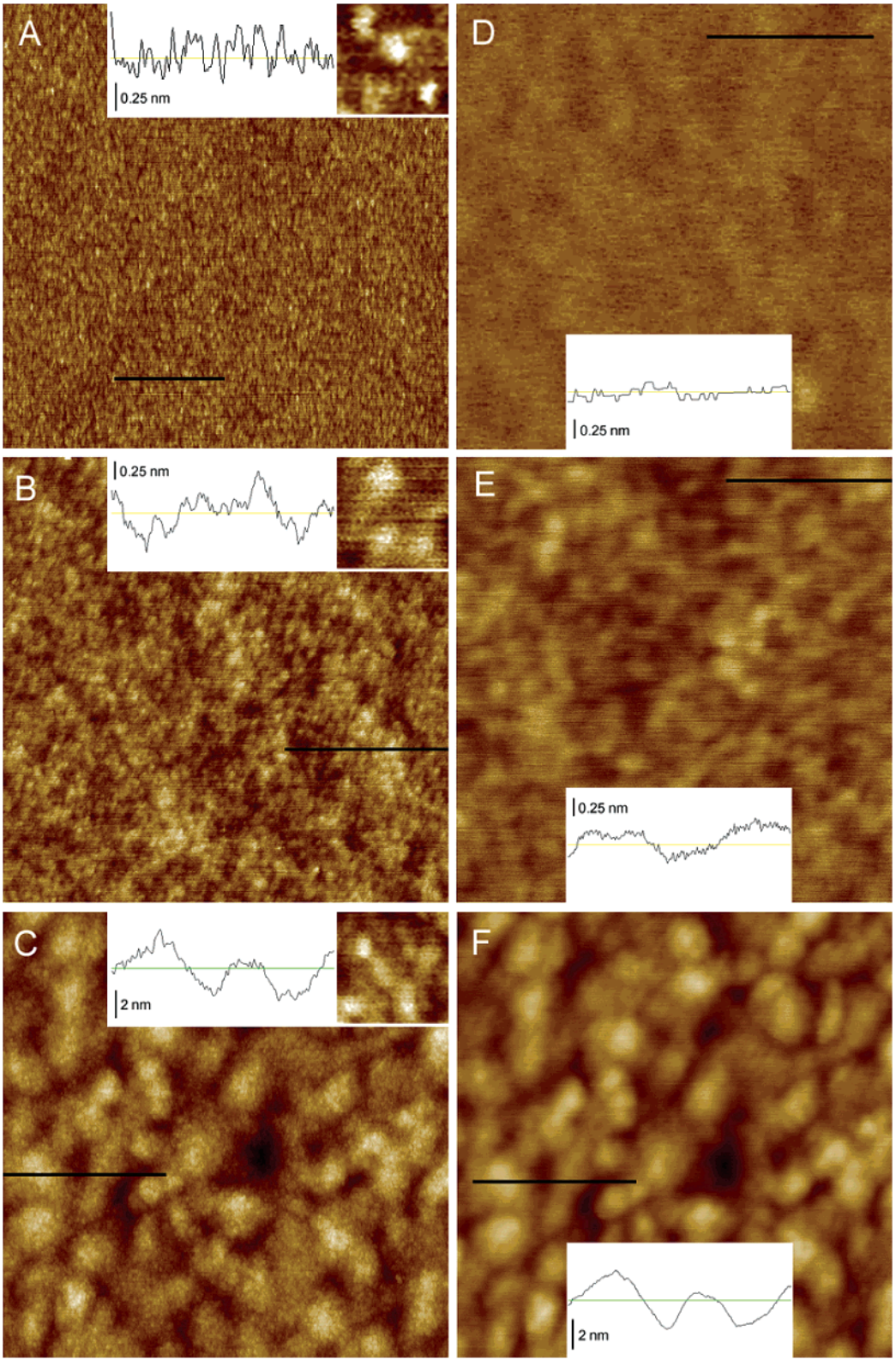

Figure 1. AFM images of UV/ozone-treated solid supports (A−C) and of DOPC/DOPS SLBs deposited on respective supports (D−F). Cross sections measured along the black lines are presented for each image. Image size, 500 nm. (A) Silicon wafer. *Z*-scale, black-to-white: 2 nm. Inset: 10× magnified view of protrusions of 3−6 nm diameter and subnanometer height (*Z*-scale, 1 nm). (B) Silica-coated wafer. Undulations of subnanometer height and lateral dimensions of ∼50 nm are observed (cross section). *Z*-scale, 2 nm. Inset: 5× magnified, showing protrusions with a diameter of 5−15 nm. Note that tip-convolution effects might enhance the lateral size of small features. (C) Silica-coated quartz crystal. Grains of 30−70 nm diameter and up to ∼5 nm height are observed, reflecting the roughness of the underlying template of evaporated gold. *Z*-scale, 10 nm. Inset: 5× magnified, revealing a subgrain structure of 3−6 nm diameter (*Z*-scale, 2 nm). (D) Silicon wafer with an SLB. Protrusions are no longer visible. *Z*-scale, 2 nm. (E) Silica-coated wafer, covered by an SLB. The surface undulations of 50 nm lateral size are still apparent, while the smaller protrusions have disappeared. *Z*-scale, 2 nm. (F) Silica-coated quartz crystal, covered by an SLB. Subgrain structures are smoothened, whereas the grains remain visible. *Z*-scale, 10 nm.

dimensions of 3−6 nm (Figure 1A, inset), the surface roughness being small (0.14 ± 0.01 nm). On silica-coated wafers (Figure 1B), both small features of 5−15 nm lateral extension (Figure 1B, inset) and faint undulations of ∼50 nm lateral scale (Figure 1B, cross section) contributed to a slightly increased roughness of 0.19 ± 0.02 nm. The surface roughness was considerably larger for silica-coated quartz crystals used for QCM-D (1.2 ± 0.1 nm). Grains with lateral dimensions of 30−70 nm and heights of 5 nm and larger could be discerned, likely to originate from the underlying template of evaporated gold (Figure 1C). In addition, a substructure with a characteristic lateral extension of 3−6 nm was resolved (Figure 1C, inset).

Imaging SLBs. We have demonstrated previously by AFM on mica[12] and by QCM-D on silica-coated quartz crystals[13] that SLBs made of DOPC/DOPS (4:1) were continuous and essentially devoid of defects. When the images at low scanning force, $F^{scan} \sim 200$ pN,[28] taken on SLB-covered substrates (Figure 1D−F) are compared with those of the bare substrates (Figure 1A−C), an important difference is revealed. Surface features of lateral dimension comparable to the thickness of a bilayer disappear (Figure 1D,E) or remain only faintly resolved (Figure 1F). The smoothening effect is manifested in decreased values for the surface roughness, being 0.06 ± 0.01 nm, 0.14 ± 0.01 nm, and 1.0 ± 0.1 nm for the silicon wafer, the silica-coated wafer, and the silica-coated quartz crystal, respectively. However, grain structures (Figure 1F) or surface undulations (Figure 1E) with lateral dimensions larger than the bilayer thickness are reproduced. The appearance of the mica surface in the presence of a bilayer did not change (not shown).

Force Measurements on Solid Supports. Force−distance curves recorded on clean supports (Figure 2A) are characteristic of solid substrates under the buffer conditions applied here.[29] Van der Waals forces and electrostatic forces are essentially balanced, resulting in small forces (<50 pN) of repulsion upon tip approach and adhesion upon tip retraction. Force curves were reproducible and independent of lateral position, tip, and applied load (up to 15 nN).

Force Measurements on SLBs. Force−distance curves on SLB-coated supports differed from what was observed on bare substrates. Typical curves are shown in Figure 2B−D for a silica-coated wafer. Three distinctive responses were obtained, depending on the load, F^{stat}, applied: (i) At low load, a first repulsive regime upon approach and no or small rupture forces ($|F^{stat}_{off}| < 0.6$ nN) upon retraction were measurable (Figure 2B). (ii) Above a threshold load, $F^{stat}_{in1} \sim 4.9$ nN in Figure 2C, the repulsive regime was followed by a jump, $d^{scan}_{in1} = 3.9$ nm (Figure 2C, arrowhead), and a second repulsive regime. Considerable pull-off forces, $F^{stat}_{off1} \sim -2.2$ nN in Figure 2C, were measured upon retraction. (iii) At loads larger than a second threshold load, $F^{stat}_{in2} \sim 12.2$ nN in Figure 2D, a second jump, $d^{scan}_{in2} = 1.5$ nm (Figure 2D, arrowhead), occurred, followed by hard-wall contact. Upon retraction, two pull-off events, $F^{stat}_{off2} \sim 1.1$ nN and $F^{stat}_{off1} \sim -1.6$ nN (Figure 2D, asterisks), could be observed.

The onset of the first repulsive regime occurs at a separation of ∼9 nm from hard-wall contact (cf. Figure 2D). This distance is close to the thickness of two lipid bilayers, indicating that apart from the bilayer on the solid support, a second bilayer must be present on the tip.

(28) The index "scan" refers to forces applied during scanning; in contrast, the index "stat" is used for forces applied in static lateral positioning of the tip with respect to the sample.

(29) Müller, D. J.; Engel, A. *Biophys. J.* **1997**, *73*, 1633−1644.

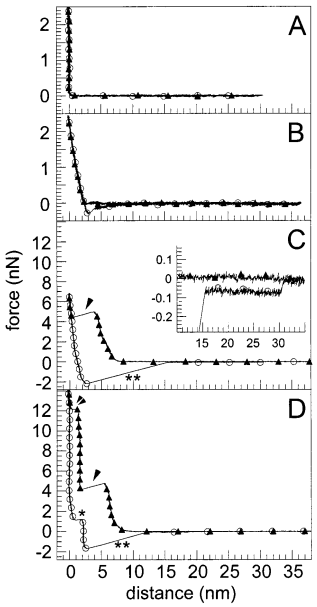

Figure 2. Force−distance curves on a silica-coated wafer without (A) and with (B−D) an SLB present, recorded in calcium-containing buffer (▲, approach; ○, retraction). No (B), one (C), or two (D) jump-in (arrowheads) and pull-off (asterisks) events can be observed, depending on the applied load. According to our interpretations, the onset of the first repulsive regime at a distance of ∼9 nm (D) is due to the presence of a second bilayer on the tip. With increasing load, the lipid material between tip and support is compressed and displaced in two sequential steps, each of them corresponding to the displacement of one bilayer. Upon retraction, a small constant negative force (C, inset) was often observed at separations beyond 10 nm, extending over several tens of nanometers, indicating that the tip can maintain some form of contact with the sample over distances exceeding the thickness of two bilayers.

The most direct interpretation of the force−distance curves presented here is that they reflect the interaction between solid supports coated by an SLB and that with increasing load, the lipid material between tip and support is compressed and displaced in two sequential steps, each of them corresponding to the displacement of one bilayer. A distance of ∼7 nm is measured between the onset of the first repulsive regime and the position after the first jump (cf. Figure 2D) corresponding to the displacement of one bilayer and subsequent compression of the remaining bilayer between tip and support.

Note that upon retraction a small constant negative force, $F^{stat}_{tub} \sim -0.06 \pm 0.05$ nN, was often observed at separations beyond 10 nm (cf. Figure 2C, inset). This force extended sometimes over distances of several tens of nanometers, indicating that the tip can maintain some form of contact with the sample far beyond separations corresponding to the thickness of two bilayers.

It was possible to switch between the three responses described above by varying F^{stat} below or above the characteristic threshold values, F^{stat}_{on1} and F^{stat}_{on2}. The qualitatively different responses persisted at varying velocities of approach and retraction (20−1600 nm/s). Forces and distances of jump-in and pull-off were reproducible with some statistical spreading (in the order of 10%).

Qualitatively similar force curves were obtained on all solid supports investigated. On mica, silicon wafers, and silica-coated wafers, the response was laterally invariant, but measured forces could vary considerably (in the order of 100%) upon exchange of the tip. Since the response was laterally invariant, we attribute these changes to the exact nature of the lipid deposit present on the tip apex and not

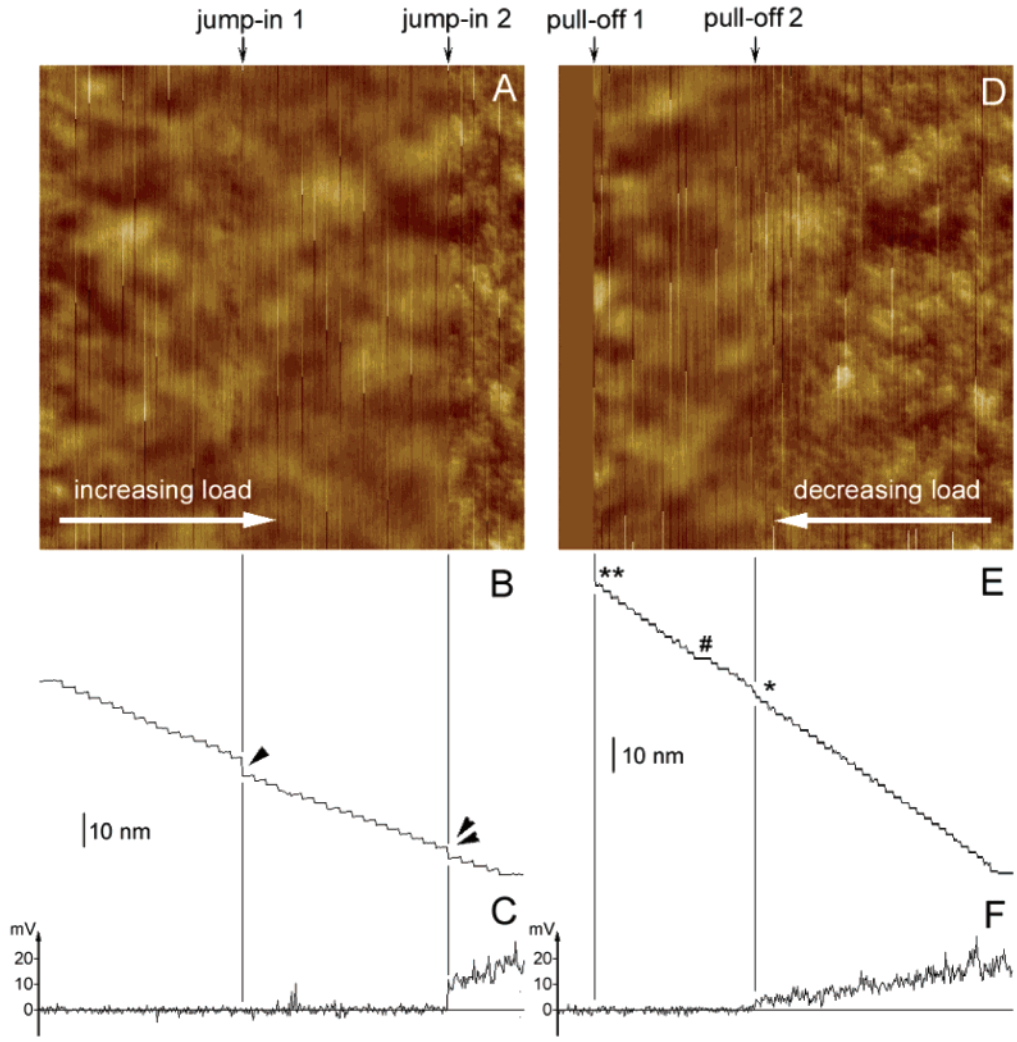

Figure 3. Effect of applied scanning force on AFM images of a lipid bilayer supported by a silica-coated wafer. The force was increased stepwise in intervals of 0.3 nN per 12 scan lines from ~100 pN to ~11 nN (A−C) and subsequently decreased in intervals of 0.3 nN per 8 scan lines until retraction of the tip (D−F). Flattened height images (A,D) were rotated by 90° with the slow scan axis as indicated by the white arrows. Cross sections of the nonflattened height images (B,E) show the *z*-movement of the scanner. The apparent regular steps of $d_{cant} = 1.6$ nm height are due to the change of the scanning force, as the scanner movement compensates for the cantilever deflection. To determine effective jump heights of the tip with respect to the substrate, d_{cant} was subtracted from heights apparent in (B) and (E). As the force was ramped manually, some irregularities did occur (# in E). (C) and (F) show friction data. (A−C) At low forces, the smooth bilayer was revealed (A) with friction below the detection limit. A first jump-in (arrowhead) of 4.0 nm at $F_{in1}^{scan} \sim 4.9$ nN did not change the appearance either of the height image or of the friction. After a second jump-in (double arrowhead) of 1.8 nm at $F_{in2}^{scan} \sim 10.2$ nN, the height image resembled that of the silica substrate and friction increased abruptly. (D,E) The friction decreased proportionally to the applied load. After a first pull-off event (asterisk) of −1.7 nm at $F_{off2}^{scan} \sim 2.6$ nN, the height image again resembled a smooth bilayer and friction was below the detection limit. The second pull-off (double asterisk) at $F_{off1}^{scan} \sim -2.8$ nN retracted the tip from the surface.

to a (permanent) reorganization of the lipid assembly induced by the tip. On silica-coated quartz crystals, however, measured forces varied laterally (in the order of 100%), likely due to geometrical constraints on the interaction between tip and substrate, imposed by the elevated surface roughness.

Force Measurements upon Scanning. To investigate dynamic aspects of the tip−sample interaction, images were recorded while the load was varied upon scanning, and responses were compared to force−distance curves acquired under static conditions.

At scanning forces, F^{scan}, used to record the images described in the above section (Figure 1), the tip immediately lost contact when decreasing the scanning force to zero. Correspondingly, force curves recorded before and after the acquisition of the images ($F^{stat} = F^{scan}$) were similar to those in Figure 2B.

To study the effect of the scanning force on the appearance of the image, F^{scan} was first increased in small regular intervals from ~100 pN to ~11 nN and then decreased until detachment of the tip from the sample, while imaging a lipid bilayer supported on a silica-coated wafer (Figure 3). Together with the height images (Figure 3A,D), friction data were also recorded (cross sections shown in Figure 3C,F) to provide complementary information about the interaction between tip and sample.

With increasing load, two steps showed up in cross sections of untreated[30] height images (Figure 3B, arrowheads), indicating abrupt approaches of the tip toward

(30) The cross sections of the untreated height image show the *z*-movement of the scanner, which can reveal jumps of the tip with respect to the distance from the substrate (Figure 3B,E, see figure legend for details); the common flattening treatment removes this information.

the substrate. The first jump-in of $d_{in1}^{scan} = 4.0$ nm occurred at $F_{in1}^{scan} \sim 4.9$ nN without significant changes in the appearance of the treated or nontreated height image, resembling an SLB (Figure 3A). The friction remained insignificant (Figure 3C). The second jump-in of $d_{in2}^{scan} = 1.8$ nm occurred at $F_{in2}^{scan} \sim 10.2$ nN. The appearance of the height image changed abruptly, resembling the underlying substrate, and the friction increased significantly. Upon further increased load, the friction increased proportionally to the applied load, whereas the topography remained unchanged.

With decreasing load, the friction decreased proportionally to the applied load. A first pull-off event of $d_{off2}^{scan} = -1.7$ nm occurred at $F_{off2}^{scan} \sim 2.6$ nN (Figure 3E, asterisk), upon which the appearance of the height image changed back to that of an SLB and the friction diminished to insignificant values. Height images and friction did not change until the tip detached entirely from the surface (Figure 3E, double asterisk), at a negative load of $F_{off1}^{scan} \sim -2.8$ nN. Correspondingly, force curves recorded with $F^{stat} > F_{in1}^{scan}$ ($F^{stat} > F_{in2}^{scan}$) were similar to those in Figure 2C (Figure 2D) showing one (two) jumps upon approach and one (two) pull-off events upon retraction. Also, friction forces measured after the second jump-in and before the first jump-off were similar to forces measured on the bare surface at comparable loads (not shown), in agreement with observations by Grant and Tiberg.[23]

When, after scanning with high loads, the tip was reapproached at low scanning force, the original image of a smooth bilayer was obtained without visible damage (not shown). Responses were reproducible upon repeated variation of the scanning force on the same area, indicating that changes in the bilayer assembly are transient. Threshold forces for jump-in (F_{in1}^{scan}, F_{in2}^{scan}) and pull-off (F_{off1}^{scan}, F_{off2}^{scan}) could deviate by 10% and 50%, respectively, whereas the jump heights could deviate by 10−20% ($n = 6$) with the same tip on the same surface. Variations were larger after tip exchange, though the qualitative response remained the same.

Taken together, three types of responses could be observed, depending on F^{scan}, which are interpreted as follows: (i) When scanning below a threshold force ($F^{scan} < F_{in1}^{scan}$) the (lipid-covered) tip is close to the SLB, following its topography, exhibiting low friction, and immediately losing contact upon decrease of F^{scan} to zero. (ii) When scanning above a threshold force ($F^{scan} > F_{in1}^{scan}$), topography and friction responses remain essentially unchanged but a jump-in event indicates that lipid material corresponding to one bilayer is displaced between tip and substrate. A negative force is required to pull the tip off the sample. (iii) When imaging above a second, yet higher threshold force ($F^{scan} > F_{in2}^{scan}$), the aspect of the height image and the friction measured indicate that the tip is close to the underlying substrate, revealing its structural details and exhibiting enhanced friction. Additional lipid material is displaced upon a second jump-in.

A remarkable adhesion mechanism keeps the tip in contact with the SLB-covered substrate in cases ii and iii. First, the adhesion does not fatigue when pulling the tip off the surface at $F_{off1}^{scan} < F^{scan} < 0 < F_{in1}^{scan}$ and $F_{off2}^{scan} < F^{scan} < F_{in2}^{scan}$, respectively. Second, the adhesion is maintained while scanning; that is, rearrangements of the lipids in the vicinity of the tip do not perturb its adhesion.

Qualitatively similar responses were obtained for SLBs on silicon wafers and mica. On silica-coated quartz crystals, some of the responses could coexist depending on the scanning force and the scanned substrate geometry. The appearance of the height image was irregular, fluctuating between SLB and substrate during one scan line and for subsequent scan lines (not shown).

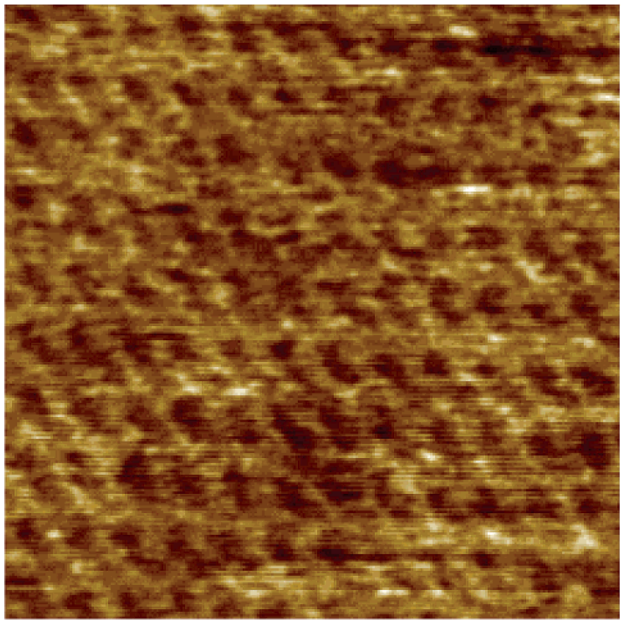

Figure 4. AFM image of a 2D crystal of streptavidin grown on an SLB of DOPC/DOPS/DPPE-lc-biotin (7:2:1) on a silicon wafer. The Fourier transform (not shown) shows diffraction peaks up to 1/2.5 nm^{-1} and confirms the c222 symmetry of the crystalline assembly as described by Reviakine and Brisson (ref 14). Image size (*z*-scale), 100 (2.5) nm.

Protein Assemblies on SLBs. The possible influence of the support roughness on the property of 2D organization of proteins on SLBs was investigated by using two model systems, streptavidin and annexin A5, which have previously been shown to form 2D crystals on mica-supported SLBs.[6,14,15,18]

2D Crystalline Assembly of Streptavidin. For streptavidin, a silicon wafer was first coated with an SLB made of DOPC/DOPS/DPPE-lc-biotin (7:2:1) in calcium-containing buffer. AFM characterization by force curves and imaging in contact mode gave responses typical of an essentially defect-free SLB (not shown). This is in contrast with results obtained on mica where numerous defects have been observed in SLBs containing biotinylated lipids.[14]

2D crystalline domains of streptavidin were observed to cover the entire surface 1 h after addition of streptavidin (40 μg/mL). Grain boundaries could be resolved (not shown). The crystalline organization was readily apparent (Figure 4) and was similar to that reported before on mica-SLBs.[14] This demonstrates that protein 2D crystals can be resolved unambiguously on bilayers formed on a support with small corrugations.

Close-Packed Assembly of Annexin A5. In the case of annexin A5, while 2D crystals form reproducibly on mica-SLBs containing 15−20% DOPS,[6,18] no 2D crystals were observed on silicon wafers or silica-coated wafers under otherwise identical conditions. Instead, a close-packed assembly of annular objects with a diameter of around 14 nm was resolved (Figure 5), the global appearance of which was stable for several hours. The annular objects can be unambiguously identified as trimers of annexin A5, which are the building blocks of annexin A5 2D crystals.[31] The

(31) Oling, F.; Bergsma-Schutter, W.; Brisson, A. *J. Struct. Biol.* **2001**, *133*, 55−63.

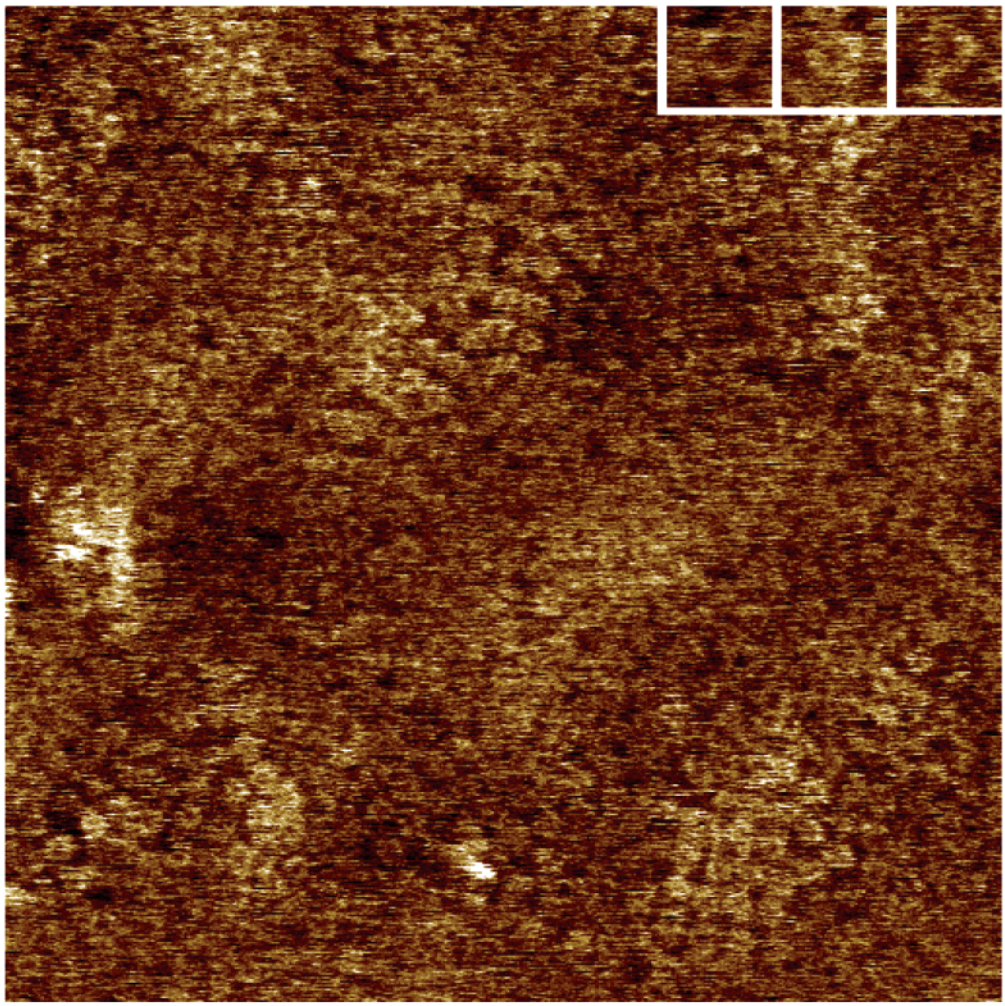

Figure 5. AFM image of the annexin A5 close-packed assembly formed on an SLB of DPPC/DOPC/DOPS (3:3:1) on a silicon wafer. The annular objects (insets) with a diameter of 14 ± 2 nm ($n = 5$) are trimers of annexin A5. No long-range order is revealed. Scan size (*z*-scale), 500 (2) nm.

difference in diameter of the objects measured here (14 nm) and by electron microscopy (10 nm)[31] is attributed to tip convolution and drifts due to the use of an O-ring. The trimers disappeared after rinsing with EDTA-containing buffer, as expected (not shown).

To investigate whether this difference originated from a lack of mobility of annexin A5 molecules on silica-SLBs, defects were created in the 2D close-packed assembly of annexin A5 trimers and the kinetics of healing of these defects was followed (Figure 6). To make defects in the protein assembly, the AFM tip was used to scan an area of (500 × 500) nm^2 of the surface with an elevated force (∼5 nN). Zoom-out images recorded at minimum force immediately afterward revealed a hole with a depth of 2.1 nm (Figure 6A). The defect was found to heal within seconds (Figure 6B,C). A subsequent zoom-in resolved the close-packed assembly of annular objects (not shown). These observations confirm that (i) the distortion of the protein−lipid assembly by the tip does not disturb the functionality of the bilayer as a *fluid* matrix for bound proteins and (ii) bound proteins can diffuse laterally in a rapid manner. Note also that a transient thin-out of the protein layer close to the defect area (arrowhead in Figure 6A) occurs immediately after scratching, which is a further indication of the high lateral mobility and thus noncrystallinity of the protein layer.

Discussion

To characterize SLBs formed on various solid supports, two types of AFM measurements were combined: force−distance curves, referred to as "static mode" as they do not involve lateral movement of the tip with respect to the support, and AFM images, referred to as "scanning mode". We show that both in static mode and in scanning mode three regimes of interaction between tip and SLBs can be obtained by operating below or above certain threshold loads, F_{in1}^{stat}, F_{in2}^{stat} and F_{in1}^{scan}, F_{in2}^{scan}, respectively. These results are interpreted according to a schematic model presented in Figure 7.

In the first regime, the tip interacts with the bilayer with little or no adhesion and slides over the bilayer (Figure 7A). In the second and third regimes, the tip indents the bilayer(s) (Figure 7B,C). These regimes are thus termed "sliding regime" (Figure 7A), "first indentation regime" (Figure 7B), and "second indentation regime" (Figure 7C), respectively. In the indentation regimes, forces, F_{off1}^{stat} (F_{off2}^{stat}) and F_{off1}^{scan} (F_{off2}^{scan}), respectively, of several nanoNewtons are necessary to pull the tip off the lipid layer. The adhesion between tip and SLB does not fatigue over time and remains upon local distortion of the bilayer induced by the movement of the tip through the bilayer. At the same time, the SLB is not permanently perturbed since the effects are reproducible. The rupture forces are expected to originate from the cohesion of the lipid

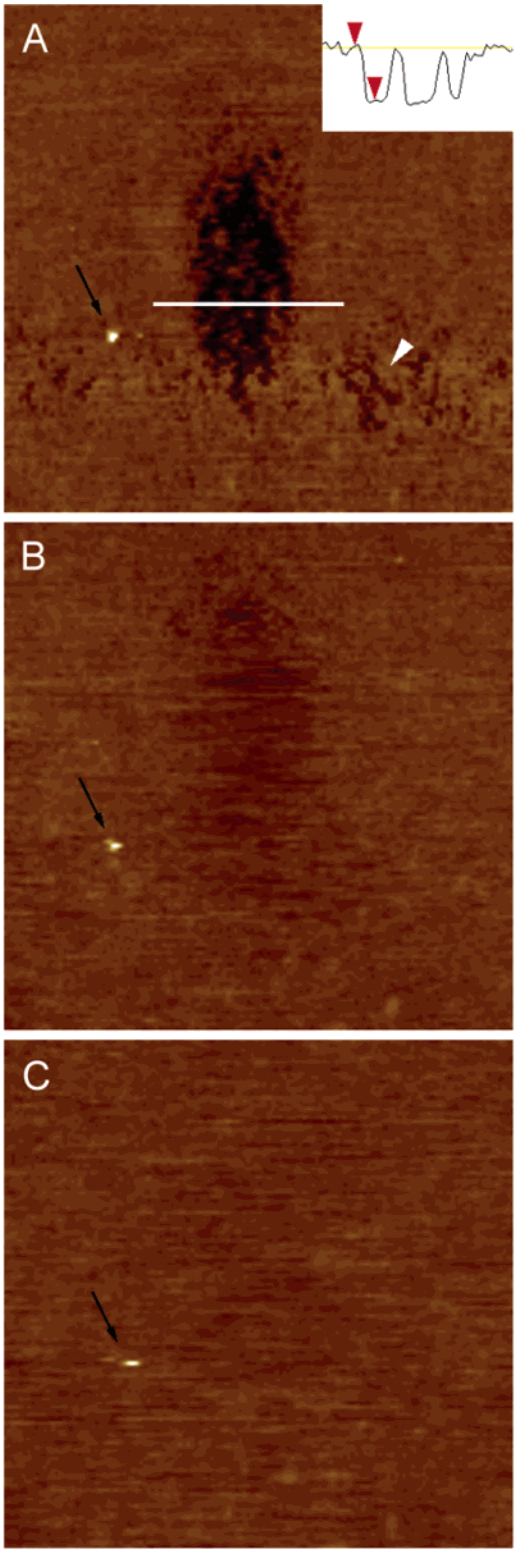

Figure 6. Healing of a defect created in a close-packed assembly of annexin A5 trimers on a lipid bilayer of DOPC/DOPS (4:1) supported on a silicon wafer. Successive images were acquired immediately (A), 20 s (B), and 40 s (C) after scratching a central area of (500 × 500) nm^2 with a force of 5 nN. The defect shows a maximum depth of 2.1 nm (cross section in (A)) and heals within seconds. As annexin A5 molecules in solution were rinsed away before scratching, healing must result from the lateral diffusion of lipid-bound annexin A5. Note a temporary thin-out of the protein layer close to the defect (white arrowhead in (A)). The contamination (black arrow) provides a reference for the lateral position. The resolution was limited to 128 × 128 pixels per image in order to decrease the image acquisition time to about 20 s. Scan size, 3 μm. *Z*-scale, 5 nm.

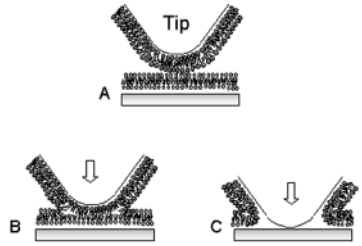

Figure 7. Schematic model representing the three regimes of tip−sample interactions described in this paper. (A) In the sliding regime, the lipid structures covering both tip and solid support remain intact. (B) A continuous lipid film with a hydrophobic interior is formed between the (moving) tip and the solid support in the first indentation regime. (C) Contact between tip and solid support is established in the second indentation regime while a continuous lipid structure is maintained around the interface of tip and support. The lipid structures are thought to be dynamic, continuously reforming upon lateral movement of the tip and stabilized by hydrophobic interactions of the lipid film.

assembly around the tip since the interaction between tip and solid support is too small to account for the measured forces.

We propose that the described regimes are associated with molecular rearrangements of the highly mobile lipids in the vicinity of the tip driven by hydrophobic/hydrophilic interactions. The simple model in Figure 7 explains our results and helps to interpret previous studies.[21,23,32] In the indentation regimes, a hydrophobic continuum is formed by the tails of the lipids, which links the tip and the substrate together (Figure 7B,C). Upon scanning, this hydrophobic continuum can move with the tip due to rapid rearrangements of the lipids, leaving an intact bilayer behind. A barrier needs to be overcome to switch between the different molecular organizations, as reflected by the threshold forces upon approach and retraction of the tip.

In addition to the molecular rearrangements driven by hydrophobic interactions, a component of mechanical compression cannot be neglected in the tip−bilayer interaction as indicated in the repulsive zones and by the fact that the jump distances do not correspond exactly to a bilayer thickness.

The mechanism proposed here is analogous to what can be observed for a hydrophilic tip interacting with a hydrophilic substrate via a water film formed by capillary forces in ambient air.[2,33] In the present case, a hydrophobic continuum is formed in a hydrophilic surrounding, held together by hydrophobic interactions, whereas the water meniscus constitutes a hydrophilic continuum in a hydrophobic surrounding (air).

The hypothesis that the silicon nitride tip is covered with lipid structures is supported by the fact that it is expected to be hydrophilic, as already reported by others.[20,23] It is thus reasonable to expect the tip apex to become covered with lipid structures once exposed to it. In the present model, the lipid assembly on the AFM tip is represented as an ideal SLB following the tip topography, although the exact organization of the lipid layer is not known and is likely to be more complex. As the tip shape and the lipid deposition are ill controlled, the conformation of the lipid assembly on the tip apex is expected to vary from tip to tip, which readily explains the variations observed for the jump-in and pull-off forces.

Double jumps or single jumps have been reported before to occur over distances corresponding to one or two

(32) Dufrêne, Y. F.; Boland, T.; Schneider, J. W.; Barger, W. R.; Lee, G. U. *Faraday Discuss.* **1998**, *111*, 79−94.
(33) Cappella, B.; Dietler, G. *Surf. Sci. Rep.* **1999**, *34*, 1−104.

bilayers, depending on the size of the AFM tip.[20,23] In addition, the hysteresis between jump-on and pull-off events has been reported previously and has received several interpretations.[21,23,32] Grant and Tiberg[23] speculate about energy dissipation during the squeeze-out of the bilayer from the contact zone, kinetically limited healing, or material trapped irreversibly in the contact zone for bilayers of DOPC and a silica tip. These reasons alone would make it unlikely for the tip to stay in the first indentation regime upon scanning at negative loads. We propose lipid rearrangements in the vicinity of the tip due to hydrophobic/hydrophilic interactions as an explanation of the observed response.

On the same lines, the formation of tubelike structures might give an explanation for forces present after retraction at distances by far exceeding the thickness of two bilayers. It is known that lipid tubes can be drawn from lipid vesicles,[34,35] and corresponding force measurements by AFM have recently been reported.[36]

The proposed mechanism is expected to occur for fluid SLBs that adsorb to support and tip. SLBs made of DOPC/DOPS (4:1) used here are indeed liquidlike as supported by the facts that (i) scratches in adsorbed noncrystalline protein assemblies heal quickly and (ii) the SLBs are defect-free and defects cannot be induced by scratching with the tip. Also, diffusion constants of $2-2.8 \times 10^{-12}$ m^2 s^{-1} [9] and $0.7-1 \times 10^{-12}$ m^2 s^{-1},[37] characteristic for fluid bilayers, have been reported for similar lipid mixtures on mica and glass, respectively. It remains to be elucidated whether a similar interaction between SLB and tip will occur with gel-phase bilayers as constrained lipid diffusion might prevent the dynamic lipid structure in the vicinity of the tip from being maintained upon scanning. However, the tip may create a local environment such that the global diffusion constant of the SLB is not the determining factor. Also the tip material used, in particular its hydrophilicity, is expected to have an influence on the interaction between tip and SLB.

The characterization of tip−sample interactions as reported here, whether in static mode (with its potential application in force mapping[29,38,39]) or scanning mode, could be particularly useful for a simple and unambiguous detection of the presence of lipid bilayers on rough supports, as standard imaging conditions involving low loads might make the detection of bilayers ambiguous. However, it was shown that the bilayer-covered silica-coated quartz crystal creates a rather complex response due to its large roughness, likely to impose geometrical constraints on the lipid-mediated tip−support interaction.

It is not entirely clear whether the images at low loads reflect the true topography of the bilayer, shown to intimately track support features larger than the bilayer thickness. It cannot be excluded that the bilayer spans over larger valleys being suspended over a limited number of protrusions but that even minimized forces exerted by the tip press the bilayer into the valley. Investigations are under way to answer this question.

Protein crystals can clearly be imaged with submolecular resolution on surfaces with small roughness such as silicon wafers and silica-coated wafers.[40,41] For rougher surfaces, for example, the silica-coated quartz crystal, this could not be done successfully. Somewhat surprisingly, the annexin A5 trimers did not crystallize on lipid bilayers supported by a silicon wafer or a silica-coated wafer under conditions where they do crystallize on a mica-SLB. This suggests that the support properties have an influence on the bilayer, which in turn has an influence on the protein crystallization process. Factors changed are the roughness of the support, even though to a small extent, and possibly the fluidity of the bilayer. The SLB clearly remains in the fluid phase, but it can be speculated that a minor change in the lipid diffusion coefficient[9,37] might influence the 2D rearrangement of membrane-bound annexin A5. Further work will aim to elucidate the origin of such variations in the 2D crystallization behavior of proteins.

Conclusions

It was shown that the AFM is a versatile tool to investigate SLBs and protein assemblies on rough surfaces. Due to a combination of imaging modes and force measurements, local properties of SLBs such as roughness or mechanical properties can be characterized. The understanding of the interactions between the SLB and the lipid-covered tip, proposed to be driven by hydrophobic/hydrophilic interactions, is crucial in order to correctly interpret the observed responses.

It could be shown that the properties of the solid support, mediated by the bilayer, can have a crucial impact on the self-organization of proteins on SLBs. This can have important consequences for the use of these systems as building blocks in biofunctional surfaces.

Acknowledgment. Discussions with Jean-Pierre Aimé and Touria Cohen-Bouhacina (University Bordeaux I, Bordeaux, France) are acknowledged. We thank Natalia Govorukhina (University of Groningen, Groningen, The Netherlands) for providing annexin A5 and Patrice Caillat and Claude Vauchier (CEA-LETI, Grenoble, France) for the gift of silicon and silica-coated wafers. Ralf Richter is the recipient of a Ph.D. fellowship from the Conseil Régional d'Aquitaine, France. This research was supported by the Conseil Régional d'Aquitaine, the Fonds Européen de Développement Régional, and EC Grants QLK2-CT2001-01339 and QLG3-CT2001-00902.

LA026427W

(34) Karlsson, M.; Sott, K.; Cans, A.-S.; Karlsson, A.; Karlsson, R.; Orwar, O. *Langmuir* **2001**, *17*, 6754−6758.
(35) Evans, E.; Yeung, A. *Chem. Phys. Lipids* **1994**, *73*, 39−56.
(36) Maeda, N.; Senden, T. J.; Meglio, J.-M. D. *Biochim. Biophys. Acta* **2002**, *1564*, 165−172.
(37) Cézanne, L.; Lopez, A.; Loste, F.; Parnaud, G.; Saurel, O.; Demange, P.; Tocanne, J.-F. *Biochemistry* **1999**, *38*, 2779−2786.
(38) Dufrêne, Y. F.; Barger, W. R.; Green, J.-B. D.; Lee, G. U. *Langmuir* **1997**, *13*, 4779−4784.
(39) Rotsch, C.; Radmacher, M. *Langmuir* **1997**, *13*, 2325−2832.
(40) Karrasch, S.; Hegerl, R.; Hoh, J. H.; Baumeister, W.; Engel, A. *Proc. Natl. Acad. Sci. U.S.A.* **1994**, *91*, 836−838.
(41) Wetzer, B.; Pum, D.; Sleytr, U. B. *J. Struct. Biol.* **1997**, *119*, 123−128.